Marine Environmental Research 178 (2022) 105643

Contents lists available at ScienceDirect

Marine Environmental Research

journal homepage: www.elsevier.com/locate/marenvrev

A multi-stable isotopic constraint on water column oxygen sinks in the Pearl River Estuary, South China

Feng Ye [a,b,*], Guodong Jia [c], Gangjian Wei [a,b], Wei Guo [d]

[a] State Key Laboratory of Isotope Geochemistry, CAS Center for Excellence in Deep Earth Science, Guangzhou Institute of Geochemistry, Chinese Academy of Sciences, Guangzhou, China
[b] Southern Marine Science and Engineering Guangdong Laboratory (Guangzhou), Guangzhou, 511458, China
[c] State Key Laboratory of Marine Geology, Tongji University, Shanghai, China
[d] Jiangxi Province Key Laboratory of the Causes and Control of Atmospheric Pollution, East China University of Technology, Nanchang, China

ARTICLE INFO

Keywords:
Oxygen depletion
Stable isotopes
Organic matter degradation
Nitrification
The Pearl river estuary

ABSTRACT

Bottom water oxygen depletion is a central concern in estuaries and coastal oceans worldwide. However, a mechanistic understanding and quantitative diagnosis of different oxygen-consuming processes are less clear. In this study, a multi-stable isotope approach is developed to delineate the role of oxygen respiration and nitrification contributing to total oxygen consumption in the Pearl River Estuary (PRE), a large eutrophic estuary in south China. The approach highly couples with analysis of the carbon isotope composition of dissolved inorganic carbon (δ^{13}C-DIC) and with stable nitrogen isotope analysis in ammonium (δ^{15}N-NH_4^+) and nitrate (δ^{15}N-NO_3^-). In all seasons, relatively low DO concentrations were observed in the upper reach and, to some extent, in the outer estuary during summer, while high concentrations of DO were found in the transition zone between the inner and outer estuary. On the basis of isotopic differentiation, our data reveal that much more depleted δ^{13}C-DIC is coincident with DIC additions and low oxygen in the upper reach and inner estuary during most seasons. This is most likely a consequence of organic carbon (OC) degradation via aerobic respiration. Based on the carbon isotopic mass balance of DIC and the stoichiometry ratio of $-\Delta DO/\Delta DIC$, we found that the OC degradation dominates the total oxygen consumption in the upper reach, as well as in the inner estuary during summer (48.3%–93.5%). In addition, nitrification is another key process in contributing to total oxygen loss in the upper reach, as supported by the well-coupled variations of δ^{15}N of NH_4^+ and NO_3^- and apparent oxygen utilization (AOU). Using the formerly determined N isotopic fractionation and observed δ^{15}N variation, we estimated that nitrification could account for 35.3%–44.1% and 28.5%–31.6% of the total oxygen consumption in the upper reach during winter and summer, respectively, while its contribution to total oxygen loss is minor in the inner and outer estuary. Overall, this study demonstrates the potential of the multi-stable isotopic approach to assess oxygen sink partitioning in large human-perturbed estuaries.

1. Introduction

Oxygen depletion is a globally significant challenge facing estuaries and coastal oceans, with severe consequences for marine life. In recent decades, the prevalence of systems that undergo hypoxic conditions (dissolved oxygen [DO] < 62.5 μmol/L) has been increasing, and future rises are anticipated due to the ongoing cultural eutrophication and global warming (Diaz and Rosenberg, 2008; Vaquer-Sunyer and Duarte, 2008; Rabalais et al., 2009). Bottom water hypoxic conditions can alter the pathways of nutrient cycling (Testa and Kemp, 2012), affect redox environments in sediments (Middelburg and Levin, 2009) and enhance coastal acidification (Cai et al., 2011). Biological oxygen consumption that reduced oxygen levels and water column stratification that acts as an effective barrier to the downward transport of oxygen-rich surface water to the bottom water are the two principle drivers that lead to the development of bottom water hypoxia in estuaries and coastal waters (Diaz and Rosenberg, 2008; Bianchi et al., 2010). Although our knowledge about the driving mechanisms for seasonal hypoxia has greatly advanced in recent years, few studies have quantitatively assessed the relative importance of multiple potential biogeochemical processes to

* Corresponding author. State Key Laboratory of Isotope Geochemistry, CAS Center for Excellence in Deep Earth Science, Guangzhou Institute of Geochemistry, Chinese Academy of Sciences, Guangzhou, China.
E-mail address: yefeng@gig.ac.cn (F. Ye).

https://doi.org/10.1016/j.marenvres.2022.105643
Received 6 February 2022; Received in revised form 3 May 2022; Accepted 4 May 2022
Available online 13 May 2022

the oxygen consumption and in turn the development of bottom water oxygen depletion, mainly due to the analytical challenges (Dai et al., 2008; Strauss et al., 2012).

From a biological perspective, biological oxygen consumption has been considered the most direct and essential condition for the development of low oxygen conditions. Among the multiple driving mechanisms, the turnover processes of carbon (C) and nitrogen (N) are highly coupled with oxygen production and consumption (see the schematic diagram in Fig. 1). Oxygen demand due to degradation of excess organic matter (OM) and high rates of nitrification reduce DO and create conditions conductive for the formation of oxygen depletion and hypoxic waters (Rabalais et al., 2009; Li et al., 2002; Dai et al., 2008; Bianchi et al., 2010). Exactly, there is an evident direct or indirect relationship between DO and DIC during OM degradation, which can be roughly characterized by the classical Redfield equation and expressed as follows (with a traditional ratio of 1.0–1.3 for –ΔDO/ΔDIC) (e.g., Redfield et al., 1963; Taylor et al., 2003; Zhai et al., 2005).

$$(CH_2O)_{106}(NH_3)_{16}H_3PO_4 + 138O_2 \rightarrow 106CO_2 + 122H_2O + 16HNO_3 + H_3PO_4 \quad (1)$$

Regarding nitrification process, it is typically carried out via the combination of two microbial processes, i.e., NH_4^+ oxidation and NO_2^- oxidation (EPA, 1993),

$$NH_4^+ + 1.5O_2 \rightarrow NO_2^- + 2H^+ + H_2O \quad (2)$$

$$NO_2^- + 0.5O_2 \rightarrow NO_3^- \quad (3)$$

The stoichiometric coefficients indicate that 1.0 mol NO_3^- addition via nitrification requires 2.0 mol of O_2 consumption.

More than concentration data alone, the measurement of stable isotopes in C and N pools provides a powerful tool to assess internal turnover and sources in estuaries and coastal oceans. Transformation processes generally favor the light isotope species (^{12}C and ^{14}N), and accordingly, the remaining substrate becomes subsequently enriched in heavy isotopes (^{13}C and ^{15}N) as turnover proceeds. For example, respiration and degradation of OM typically produces DIC with minor isotope fractionation from the OC substrate, and therefore adds ^{13}C-depleted respiratory CO_2 to the total DIC pool. Nitrification is unique to some extent, because it is a two-step with divergent isotope effects. The first step, NH_4^+ oxidation, is associated with a large ^{15}N fractionation (ε = 14–38‰), and thus could increase $\delta^{15}N$ of the residual NH_4^+ but add isotopically depleted NO_2^-/NO_3^- along with oxygen consumption (Cifuentes et al., 1989; Casciotti et al., 2003). The second step, NO_2^- oxidation, exhibits an inverse fractionation (ε = −12.8‰) (Casciotti, 2009). The newly produced NO_3^- is heavier than the source NO_2^-, and the residual NO_2^- becomes progressively depleted in ^{15}N during NO_2^- oxidation. Based on isotope changes of multiform C and N and their link to oxygen data, in combination with the associated isotope effects during biogeochemical processes, it is possible to study the oxygen dynamics and quantify the contribution of different biogeochemical processes on oxygen sinks (Strauss et al., 2012; Wang et al., 2016; Wells and Eyre, 2019). For example, using the stable C isotope coupled with a three end-member mixing model, Wang et al. (2016) demonstrated that the summer hypoxia in bottom waters of Changjiang plume could be predominately attributed to decomposition of biomass produced by overlying phytoplankton, as the $\delta^{13}C$ value (−18.5 ± 1.0‰) of the remineralized OC was very similar to the $\delta^{13}C$ of marine sourced POC produced in situ (−18.5 ± 0.3‰).

Oxygen depletion (<94 μmol/L) or even seasonal hypoxia are frequently occurred in the Pearl River Estuary (PRE), a large subtropical estuarine system in south China that has been under massive anthropogenic pressure (e.g., Yin et al., 2004; Zhang and Li, 2010; Ye et al., 2013; Qian et al., 2018). The largest corresponding <62.5 μmol/L hypoxic zone reported was ~660 km^2 in the summer of 2014. High rates of OM decomposition, both from external sources or in situ OM caused by excess nutrient inputs, and strong water column stratification are the two primary mechanisms responsible for the occurrence of bottom water oxygen depletion (Yin et al., 2004; Dai et al., 2008; Qian et al., 2018; Zhao et al., 2020). Other factors contributing to the variations of DO include estuarine circulation, bottom topography and bottom water residence time (Yin et al., 2004; Ye et al., 2013). Previous studies have mainly addressed the physical mechanisms responsible for the variations of DO and the formation of hypoxia in the PRE. In contrast, the biogeochemical sources and sinks of DO are poorly constrained and understood. The few published work on oxygen consumption rates are confined to the upper reach and discrete sampling stations within the estuary (Chen et al., 2004; He et al., 2014). According to previous studies (Rabouille et al., 2008 and references therein), the oxygen consumption rates in the PRE are comparable or even higher than the most severe hypoxic zones in the world (e.g., the northern Gulf of Mexico and Chesapeake Bay, USA). For example, aerobic respiration and

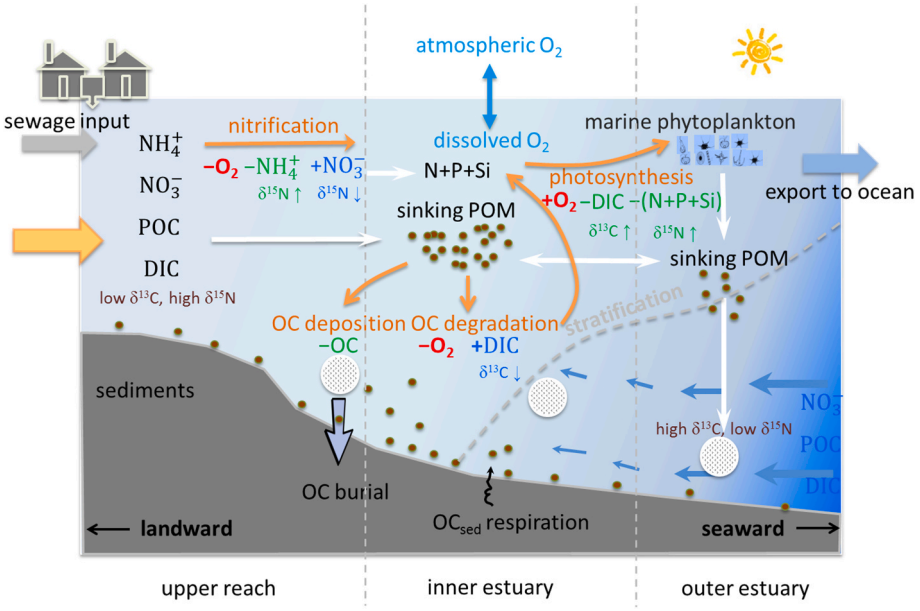

Fig. 1. A conceptual model for multi-carbon and nitrogen stable isotopic constraints on water column oxygen sinks in estuaries and coastal oceans.

nitrification substantially contributed to the oxygen depletion in the upstream region, among which nitrification can account for one third of the total community oxygen consumption in the upmost station during wet seasons (Dai et al., 2006, 2008). In recent years, the $\delta^{13}C$ of DIC has been used to explore the relative contribution of aerobic respiration of OM to total oxygen loss in bottom waters of the PRE during the summertime (Su et al., 2017; Zhao et al., 2020).

In this article, we evaluated multiple potential mechanisms responsible for reducing oxygen levels in the Pearl River Estuary from a biogeochemical perspective, and quantified the relative effects of these drivers using a suite of isotopic measurements and mixing models. Based on the tight coupling of organic (inorganic) carbon-reactive nitrogen-oxygen dynamics and the associated isotopic variations with oxygen consumption, we aimed to (1) delineate whether the developed isotopic-metric is possible to trace the DO sources/sinks in the water column, and (2) gain further insight into the relative importance of aerobic respiration and nitrification in leading bottom water oxygen consumption, especially during the summer periods when low oxygen conditions generally occur. To the best of our knowledge, this is the first study to understanding the role of OM decomposition and nitrification-induced oxygen consumption in controlling oxygen dynamics based on in situ measurements of multiform C and N isotope.

2. Materials and methods

2.1. Study area

The Pearl River Estuary (PRE) is a bell-shaped subtropical estuary in southern China with a mean depth of 4.8 m (maximum water depth of >20 m) and a surface area of almost 2000 km^2. The estuary is a typical freshwater-dominated estuary with weak tides (<1 m at the estuary mouth) (Dong et al., 2004). It receives the majority of fresh water from the Pearl River (PR), which has three major branches (West River, North River and East River) and several small net-like branches in the delta. Approximately 80% of the river discharge occurs in the wet season from April to September. During wet periods, estuarine mixing conditions are largely controlled by elevated river discharge and southwesterly prevailing winds, and water column stratification generally forms. During dry periods, the estuary is in general partially mixed due to the reduced river flow and strong northeast winds. The residence time for freshwater is about 2–3 days in wet seasons, but can be prolonged to 1–2 weeks in dry seasons (Dong et al., 2009; Sun et al., 2014).

Over the last 3 decades, the PRE has experienced an increased nutrient load as a result of the intensification of agricultural practices and growing urbanization in the catchment area. The concentration of dissolved inorganic nitrogen (DIN, the sum of NO_3^-, NO_2^- and NH_4^+) from the Pearl River has increased 3-fold in the past 30 years (Ning et al., 2009). Excess nutrient inputs to the estuary result in increasing primary productivity (Harrison et al., 2008). Phytoplankton biomass, together with terrestrial OC loads, flux OM to the seafloor and being oxidized by bacteria, thereby triggering rapid dissolved oxygen consumption in the water column. Consequently, low oxygen waters or even hypoxic conditions generally occur, especially during the summer season when vertical stratification forms (Yin et al., 2004; Ye et al., 2013; Qian et al., 2018). Moreover, the sediment load declined drastically since the early 1990s, due mainly to the construction of dam in the drainage basin (Zhang et al., 2008; Wu et al., 2019). As a consequence, there has been a shift toward more contributions of biological reactive algal biomass to total POC within the estuary (Liu et al., 2012; Guo et al., 2015).

2.2. Water sampling and sample analysis

Sampling was performed along the salinity gradient of the PRE on the boat Yue-Dongguan-Yu 00589 in each season: autumn (November 2013), winter (February 2014), spring (May 2014) and summer (August 2014). According to their geographic distributions, previous studies generally divided the sampling locations into three zones, i.e., the upper reach (upstream of the Humen outlet), inner estuary and outer estuary (Fig. 2, Guo et al., 2008; Ye et al., 2016). Temperature and salinity were obtained using a Valeport mini-CTD (conductivity-temperature-depth) probe. At each site, water samples were collected using 5 L Niskin bottles from both surface (~0.5 m below the air-sea interface) and near bottom (~1 m above the bottom). Following collection, each water sample for isotopic analysis was filtered through a pre-combusted (450 °C) GF/F membranes (nominal pore size 0.7 μm). The filtrate was flash frozen with liquid N_2 and kept at −20 °C until further analysis. The filters for particulate matter determination were rinsed with Milli-Q water to remove sea salt and then immediately stored frozen. The chlorophyll *a* (Chl *a*) samples were stored frozen in the dark until analysis. DO concentrations were measured using the Winkler titration method with a precision of 2.1 μmol/L (Strickland and Parsons, 1972). Apparent oxygen utilization (AOU) was calculated by the difference between the measured DO and the saturated DO with the same physical and chemical conditions.

Nutrient concentrations, including NO_3^-, NO_2^- and NH_4^+, were analyzed on autosampler system using the standard colorimetric techniques, after the frozen samples were thawed under tap water. The precision of the analyses was better than 3% for three N species (Ye et al., 2016). The N isotopic composition of nitrate ($\delta^{15}N$-NO_3^-), nitrite ($\delta^{15}N$-NO_2^-) and ammonia ($\delta^{15}N$-NH_4^+) was analyzed by the chemical conversion method based on procedures outlined in McIlvin and Altabet (2005) and Zhang et al. (2007), respectively. In brief, various N species are quantitatively converted to N_2O using sodium azide in an acetic acid buffer, after reduction/oxidation processes. The resultant N_2O gas was purified and collected on a TraceGas preconcentration system, followed by isotopic analysis on an isotope ratio mass spectrometry (IsoPrime 100, Elementar Inc.). Isotope values are reported in delta notation (δ) in units of per mil (‰) as follows:

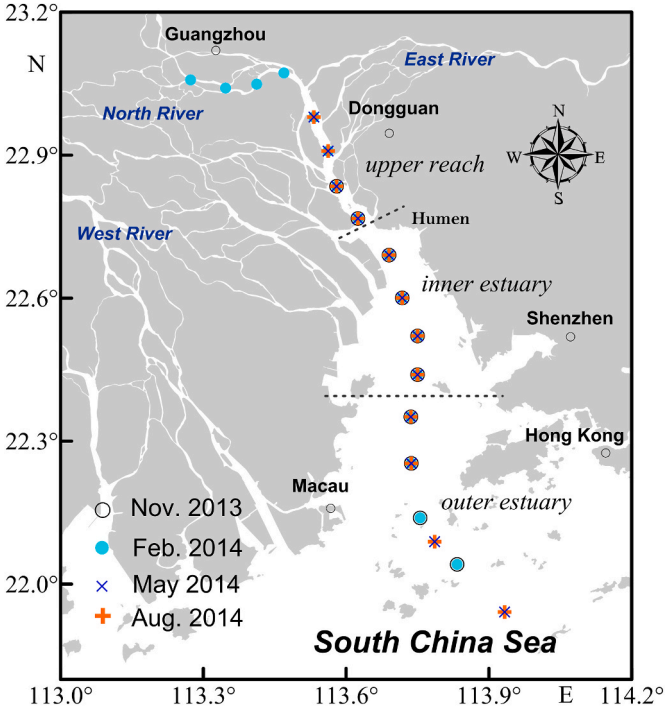

Fig. 2. Map of the Pearl River Estuary showing the sampling stations. This study divided the estuary into three zones: (1) upper reach; (2) inner estuary; and (3) outer estuary.

$$\delta^{15}N = \left(\left[\left(\frac{^{15}N}{^{14}N}\right)_{sample} \Big/ \left(\frac{^{15}N}{^{14}N}\right)_{standard}\right] - 1\right) \times 1000$$

Measurements were referenced to Air N_2 (for $^{15}N/^{14}N$) using internationally certified standards (NO_3^-: USGS-32, USGS-34 and USGS-35; NH_4^+: IAEA-N1, USGS-25 and USGS-26). For NO_2^- isotope analysis, we used two in-house nitrite standards with known $\delta^{15}N$ values (Lab1: $\delta^{15}N$ = 0.9‰ and Lab2: $\delta^{15}N$ = −11.8‰) which were determined via EA/IRMS analysis. The analytical precision for nitrate samples was better than 0.3‰ for $\delta^{15}N$ and 0.5‰ for $\delta^{18}O$ (n = 8). For NH_4^+ samples, the analytical precision of $\delta^{15}N$ values was generally better than 0.4‰.

Dissolved inorganic carbon (DIC) was determined by acid extraction using a total organic analyzer (TOC-L, Shimadzu Corporation, Kyoto, Japan), using the total inorganic carbon mode. The precision of the method is 2.0 μmol kg^{-1} for DIC. The $\delta^{13}C$-DIC and $\delta^{13}C$-POC values were determined using a Gasbench IIextraction line coupled with an isotope ratio mass spectrometer (IRMS, Delta V Advantage) and an elemental analysis-IRMS (Delta XL Plus EA-IRMS) respectively, and more detailed analytical procedures are described in Guo et al. (2015). The $\delta^{13}C$ values are given as per mil (‰) deviations from the standard Vienna Pee Dee Belemnite (VPDB), i.e.,

$$\delta^{13}C = \left(\left[\left(\frac{^{13}C}{^{12}C}\right)_{sample} \Big/ \left(\frac{^{13}C}{^{12}C}\right)_{VPDB}\right] - 1\right) \times 1000$$

The standard deviation for the international and in-house standards was 0.2‰ for $\delta^{13}C$-DIC and 0.1‰ for $\delta^{13}C$-POC, respectively. The deviations for the replicate samples were in the same range or better. Note that much of data in surface waters including the concentration and isotopic composition of DIC/POC and NO_3^-/ NH_4^+ during summer and winter seasons has been published previously (Guo et al., 2015; Ye et al., 2016).

2.3. Data analysis

To examine the sources and turnover of carbon and nutrients in the Pearl River Estuary, we evaluate the mixing pattern of these constitutes (both concentration and stable isotope) along the salinity gradient by using a two end-member mixing model, comparing them to conservative mixing. As the marine end-members, we selected the offshore surface water for DIC and relative stable subsurface water (100–200 m) from the northern South China Sea (NSCS) for DIN, rather than the samples with highest salinities (Ye et al., 2016; Zhao et al., 2020). Because the Pearl River is composed of three main branches with complex net-like small rivers in the estuarine zone (Fig. 1), it is difficult to decide a common freshwater end-member at present. Alternatively, we note that the distributional patterns of multiple C and N pools as well as their stable isotopes varied greatly at an early stage of estuarine mixing in all seasons, suggesting that beyond this point, no significant freshwater mixing between tributaries and/or anthropogenic input can be identified. In the wet season, the mixing mainly occurs in the inner estuary near Humen outlet, so we use the sampling station located in the upmost part of the inner estuary as the riverine end-member; in the dry season, the mixing mainly occurs at the upper Humen area, so the data of station after mixing with East River was used as the end-member. We note that these are not truly riverine end-members because they also reflect the influence of multiple biogeochemical processes that may have occurred in the low-salinity regions. A summary of the end-member values used in this study is listed in Table 1. More details of the riverine end-members can be found elsewhere (Guo et al., 2008; Ye et al., 2016).

Regarding the salinity distributions of concentration and isotope patterns, we divided the salinity gradient into three zones termed (L) low-salinity zone (<3.0), (M) the intermediate-salinity waters, and (H) high-salinity zone (S > 20–25). In the dry season, the low-salinity zone is found in the Guangzhou channel of the upper reach, whereas the intermediate-salinity and high-salinity waters are found in the lower section of the upper reach as well as inner estuary and outer estuary, respectively. In the wet season, however, the low-salinity zone is nearly consistent with the region of the upper reach, while the intermediate-salinity occupies most of the inner and outer estuary. In fact, similar to that of DIC concentration (Cai et al., 2004; Guo et al., 2008), if we extended the conservative mixing line of $\delta^{13}C$-DIC to zero salinity, we can obtain the effective riverine $\delta^{13}C$-DIC. The $\delta^{13}C$-DIC values of −7.5‰ and −10.3 to −10.2‰ can be estimated during the dry and wet periods, respectively. These values are consistent with the average $\delta^{13}C$-DIC recently reported in the Pearl River Delta (Xuan et al., 2020).

The mixing behavior of compounds can be assessed using the following classical mixing model:

$$X_{cons} = X_R \times f_R + X_M \times (1 - f_R) \quad (4)$$

$$\delta_{cons} = \frac{\delta_R \times X_R \times f_R + \delta_M \times X_M \times (1 - f_R)}{X_{cons}} \quad (5)$$

where X and δ denote concentration and isotopic composition, the subscripts R and M indicate composite riverine and marine end-members respectively, f denotes the fraction of riverine in each sample calculated from salinity:

$$f_R = 1 - \frac{S_{sp} - S_R}{S_M - S_R} \quad (6)$$

where sp refers to the salinity of sample.

By comparing each measured concentration and isotopic composition of DIC and NO_3^- to that expected from conservative mixing, the deviations from mixing can be defined as,

$$\Delta X = X_{meas} - X_{cons} \quad (7)$$

$$\Delta\delta = \delta_{meas} - \delta_{cons} \quad (8)$$

The difference (Δ) between the measured and conservative constituents represents the magnitude of the biological alternation and/or physical sediment-water interaction and/or air-sea gas exchange (for DIC).

The spatial and seasonal variation of DO, multi-form C and N concentrations and isotopic composition and other relevant parameters were plotted using the software Grapher 10. Relationships between DO or AOU and these parameters were analyzed with the Pearson correlation. All statistical analyses were carried out at a significance level $p < 0.05$ and were performed with the software SPSS16.0 for windows.

Table 1
Definitions of the riverine and marine end-members in the present study.

Endmember	Season	Salinity	DIC (μM)	(μM)	NH_4^+ (μM)	$\delta^{13}C_{DIC}$ (‰)	$\delta^{15}N_{NO3}$(‰)
Riverine	autumn	2.4	1.65	85.00	22.80	−7.50	6.60
	winter	5.5	2.20	75.00	30.00	−6.30	−0.90
	spring	1.6	1.50	75.00	21.60	−9.70	5.00
	summer	3.0	1.60	70.40	2.20	−8.90	5.70
Marine	all seasons	33.7 (DIC) 34.5 (DIN)	1.92	5.00	0.01	0.80	4.00

3. Results

In the upper reach (i.e., upstream of the Humen outlet), DO concentrations were mostly undersaturated, ranging between 73 and 238 μmol/L, coinciding with high phytoplankton biomass (as indicated by *Chl a* concentration), particularly in the warm summer (Fig. 3). However, low oxygen conditions (<94 μmol/L) appear to occur over a limited area during the sampling period. In the inner estuary where SPM concentrations were high, DO increased downstream with salinity and amounted to 10–20% over the saturation level in dry periods. Further downstream with high-salinities (S > 20–25), the O_2 concentrations remained stable in surface waters but dropped to less than 135 μmol/L in bottom waters of the summer cruise. DO exhibited strong vertical variations, with much higher concentrations at the surface and lower values at the bottom. This was particularly evident in the outer estuary during wet seasons.

The physiochemical characteristics showed significant seasonal variations in the PRE (Fig. 3). During wet periods, the freshwater endmember (S < 1) was located 0–20 km upstream of Humen in the upper reach, but it moved to 40–60 km upstream of Humen in dry periods. The spatial distribution of salinity was highly variable but generally increased seaward, which is typical of a freshwater-dominated estuary with weak tides and a clear interface between freshwater and seawater. The water column was well mixed in most of our study area. In contrast, the salinity data from the outer estuary showed a notable stratified water column during the wet season, with warm and fresh surface water but cool and more saline water at the bottom. Highest concentrations of total suspended matter (SPM) were observed in the freshwater during most seasons (winter, spring and summer), with a second maximum in the transition between the inner and outer estuary. In autumn, SPM concentrations in the mixing zones were higher (>40 mg/L) than those in both landward and seaward sampling stations (<25 mg/L). On all four cruises, the highest *Chl a* contents were observed in the upper reach, especially in winter and summer. They generally declined with increasing salinity, but a second maximum is visible in the inner estuary during some cruises.

The spatial distribution of concentrations and isotopic compositions of DIC and DIN forms (NO_3^-, NH_4^+ and NO_2^-) along the flow direction of the PRE are shown in Figs. 4 and 5, whereas along the salinity gradient of the estuary are shown in Figs. 6 and 7. DIC exhibited a strong seasonal and spatial variation, with much higher concentrations in dry seasons than wet seasons for the near freshwater samples. In the wet season, DIC increased seaward with increasing salinity but with a nonlinear relationship in the low salinity zone (i.e., the upper reach), whereas it exhibited an opposite pattern in the dry season. DIC was mostly conservative in the salinity range from 3 to >30 in all seasons, but with some notable deviations in middle to high salinity during both summer and winter. The distribution pattern of DIC is consistent with previous investigations in the PRE (Cai et al., 2004; Guo et al., 2008). The concentrations of all inorganic N forms were relatively high in the upper reach. The average DIN concentrations were much higher in the dry season than in the wet season. It should be noted that there was a

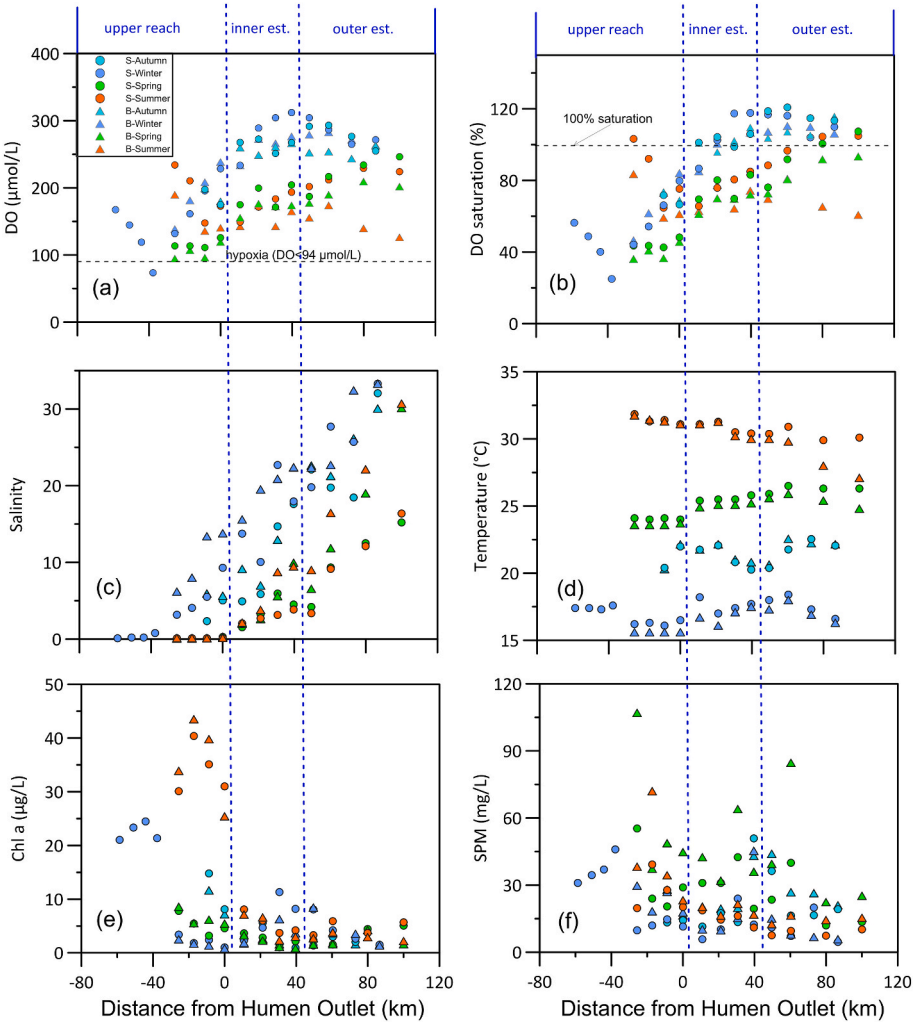

Fig. 3. Seasonal variation of DO and other physiochemical characteristics along the estuary.

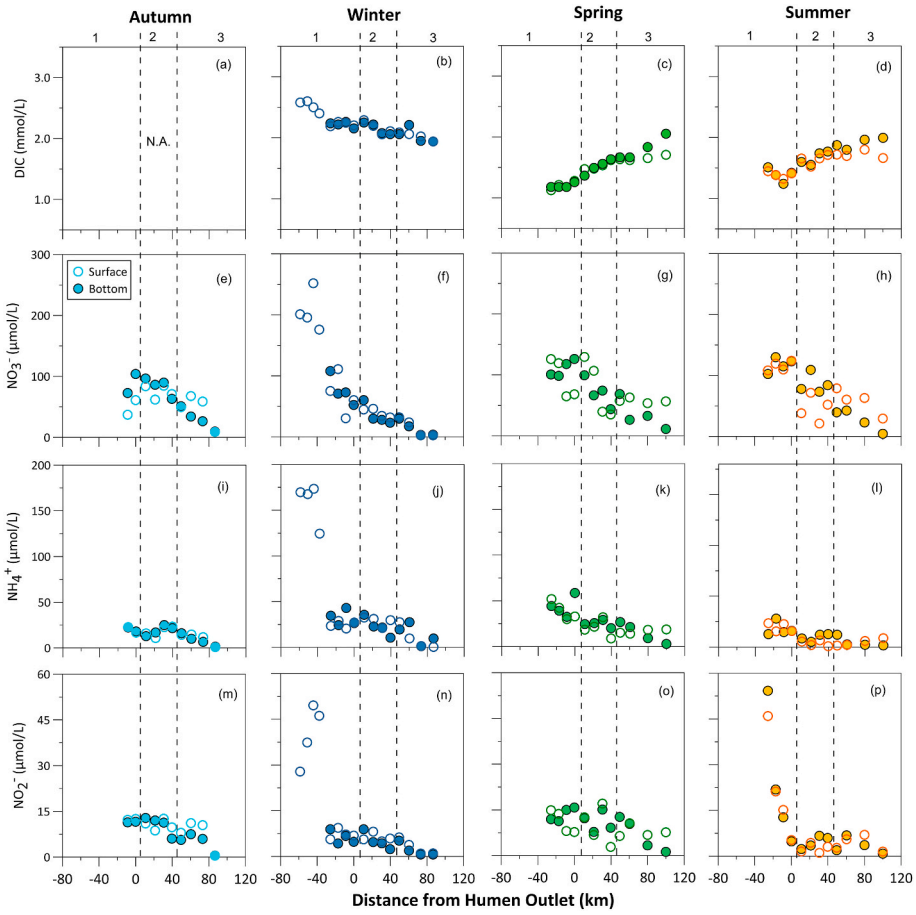

Fig. 4. The concentrations of surface and bottom DIC, NO_3^-, NH_4^+ and NO_2^- versus distance from the Humen outlet. The number 1, 2, 3 illustrate the upper reach, inner estuary and lower estuary.

significant decrease in [NH_4^+] but an increase in [NO_3^-] in the same region, coincident with the sharp decrease in DO. Concentrations thereafter decreased sharply in the low-salinity zone during all four cruises. Further downstream, concentrations of different N forms decreased steadily and were mostly conservative with increasing salinity. However, significant deviations falling above the conservative mixing line were seen in the estuarine mixing waters, in particular during the dry periods.

The δ^{13}C-DIC values ranged from −11.8 to 0.3‰ for the samples analyzed in this study. The near freshwater ($S < 1.0$) in the upper reach generally have much lower δ^{13}C-DIC values than the waters collected from the outer estuary (Fig. 5). The δ^{13}C-DIC in the near freshwater was lowest during the springtime, and increased nearly conservative downstream with increasing salinity. In contrast, the DIC in the upper reach is slightly more enriched in ^{13}C during other seasons, but decrease downstream in the low salinity waters. Low δ^{13}C-DIC values were found near Humen outlet during most seasons (i.e., autumn, spring and summer). However, measured δ^{13}C-DIC values were lower than that expected from conservative mixing for a significant number of samples in the estuarine mixing zone (Fig. 7). Further offshore, the δ^{13}C-DIC pattern can be largely explained by the freshwater-seawater mixing.

The δ^{15}N composition of different DIN forms exhibited strong spatial and seasonal variation (Fig. 5): (1) they are much more variable during winter than wet periods, (2) the average δ^{15}N-NO_3^- values were much higher in the wet than the dry seasons (5.5–6.7‰ vs. 2.7–4.8‰), whereas the δ^{15}N-NH_4^+ has an opposite pattern (2.0–7.8‰ vs. 9.7–20.1‰). (3) With respect to the spatial (salinity) distribution, δ^{15}N-NO_3^- decreased sharply in the upper reach with low salinity ($S < 3$), where a dramatic increase in [NO_3^-] associated with decreasing oxygen was found. These variations are associated with a continuously increasing enrichment in ^{15}N of NH_4^+ but a marked decrease in [NH_4^+]. Further downstream, the δ^{15}N-NO_3^- remained stable and behaved almost conservatively up to a salinity of 20–25 during wet seasons, but largely distributed below the conservative mixing line in dry seasons (Fig. 7) when elevated [NO_3^-] and high concentrations of SPM were observed, and then increased in the most saline sample in all seasons. For the δ^{15}N of NH_4^+, it decreased steadily from the lower section of the upper reach to outer estuary in the dry period, but exhibited little variation within the estuary in the wet period. Outliers with δ^{15}N-NH_4^+ ([NH_4^+]) falling below (above) the mixing line are remarkable at the intermediate salinity waters (between the inner and outer estuary) during dry periods (Figs. 6 and 7), seems to indicate an additional input of ^{15}N-depleted NH_4^+, which will be discussed later in section 4.2. Throughout entire estuarine gradient, however, it is difficult to understand the real mixing curve. Values of δ^{15}N-NO_2^- are more variable than both of δ^{15}N-NO_3^- and δ^{15}N-NH_4^+ in most seasons, with the exception of spring when the δ^{15}N of all N forms are relatively stable along the salinity gradient.

In the surface water, a positive correlation could be only established between AOU and δ^{15}N-NH_4^+ during the winter cruise, if all data points pooled together. However, in the bottom water, a significant positive relationship ($p < 0.01$) can be found between AOU and δ^{15}N-NH_4^+ in all seasons except spring when a negative relationship was observed (Figs. 8 and 9). In contrast, there were no relationships between AOU and δ^{15}N of NO_3^- ($p > 0.05$) in both surface and bottom waters. When the data points were pooled separately based on their geographic locations, we found significant positive relationships ($p < 0.01$) between δ^{15}N-NH_4^+ and AOU in the upper reach during winter and summer, a negative

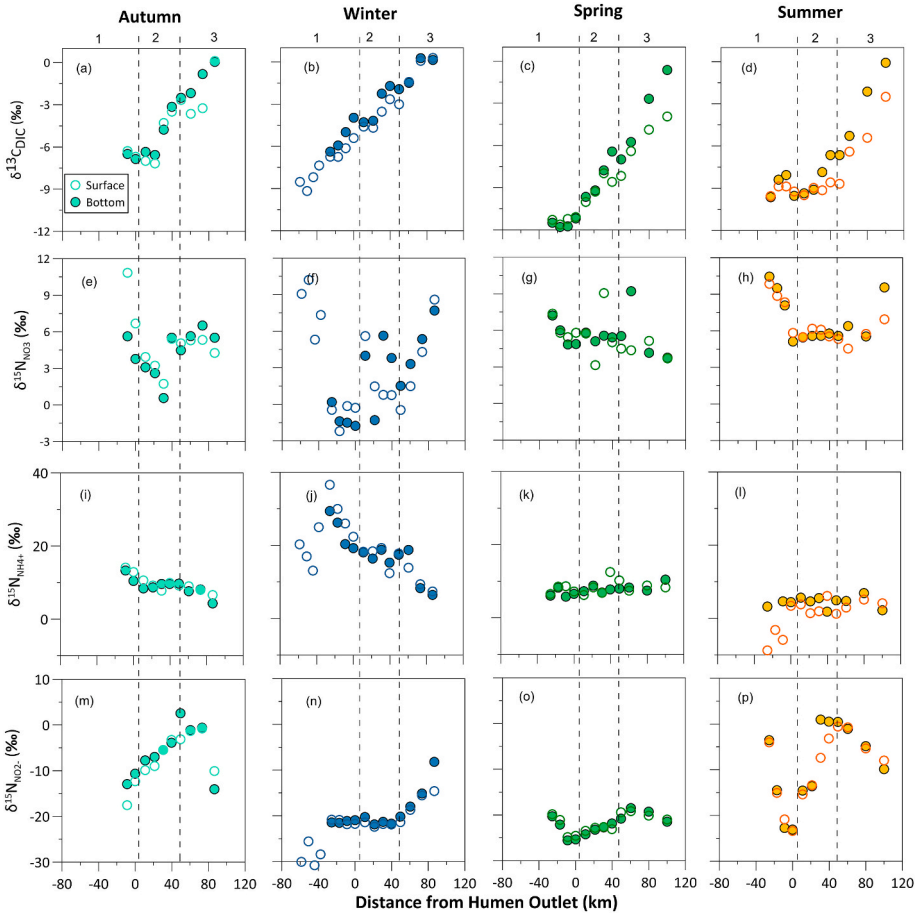

Fig. 5. The isotopic composition of surface and bottom DIC, NO_3^-, NH_4^+ and NO_2^- in both surface and bottom water samples versus distance from the Humen outlet. The number 1, 2, 3 illustrate the upper reach, inner estuary and lower estuary.

correlation in the surface waters of the outer estuary in most seasons, whereas no such relationship was observed in the inner estuary in all seasons. Among the four sampling seasons, winter and summer were the seasons when the $\delta^{15}N$ of all forms correlated ($p < 0.05$), although the direction of correlations varied from negative ($\delta^{15}N\text{-}NO_3^-$ vs. $\delta^{15}N\text{-}NH_4^+$ and $\delta^{15}N\text{-}NO_2^-$ in summer, and $\delta^{15}N\text{-}NH_4^+$ vs. $\delta^{15}N\text{-}NO_3^-$ and $\delta^{15}N\text{-}NO_2^-$ in winter) to positive ($\delta^{15}N\text{-}NO_3^-$ vs. $\delta^{15}N\text{-}NO_2^-$ in winter and $\delta^{15}N\text{-}NO_2^-$ vs. $\delta^{15}N\text{-}NH_4^+$ in summer). The relationships between DO and different environmental parameters can be also found in Figs. S1–4.

4. Discussion

4.1. Isotopic evidence for oxygen consumption due to aerobic respiration

While the mixing between riverine water and seawater dominated the distributions of DIC concentrations and nutrients in the PRE (Fig. 6), a number of other processes are clearly important as well, and may explain the deviations from conservative mixing. In most cases, the major processes moderate the non-conservative behavior of DIC in estuaries including biological metabolism, intense physical sediment-water interaction and resuspension of sediments, tributary and local anthropogenic inputs (Cloern et al., 2002; Wu et al., 2003). Among these processes, net biological production (with DIC removal and DO gains) and aerobic respiration (with DIC additions and DO loss) are highly associated with estuarine oxygen dynamics. In the following, we try to distinguish the effects of one from the other in controlling the non-conservative behavior of DIC and its $\delta^{13}C$ in this subtropical estuarine system.

The upper reach had very high concentrations of OC and nutrient in the near freshwater area ($S < 1$). The well coupled signals of decreased $\delta^{13}C$-DIC and low oxygen (Figs. 3 and 5), together with the strong OM degradation signal (POC and *Chl a*), allow us to suggest that aerobic respiration may play a crucial role in controlling oxygen dynamics in this region. In most cases, the DIC produced by the degradation of OM via aerobic respiration inherit light ^{13}C signals from OC and will therefore add isotopically light DIC to the system. It is interesting to note that the riverine $\delta^{13}C$-DIC in spring exhibited much lower values than other seasons (−12 to −11‰ vs. −10 to −7‰), when oxygen concentrations were also low (Figs. 3 and 5). This suggests that the spring DIC may have originated primarily from the weathering of carbonate rocks in the early flood season (Guo et al., 2015). The much higher $\delta^{13}C$-DIC (−10 to −8‰) measured during summer compared to other seasons are probably due to an enhanced biological uptake (i.e., photosynthesis), either in situ or transported from upstream, as indicated by the high phytoplankton biomass and DO concentrations (Fig. 3). A clear seaward decrease in $\delta^{13}C$-DIC was seen during autumn and summer (Fig. 5). This decrease was accompanied by significant additions of DIC but removal of POC (Guo et al., 2015), clearly suggesting the regeneration of DIC from OM degradation. Further downstream in the low-salinity waters ($1 < S < 3$, i.e., in the lower section of the upper reach in the dry season, but in the inner estuary in the wet season), there was a substantial change in $\delta^{13}C$-DIC (Fig. 7). This, in conjunction with a rapid decline in the concentrations of most constituents (e.g., POC and nutrients), could be due to the complicated freshwater mixing of different tributaries in the upstream (e.g., Guo et al., 2008; He et al., 2014; Guo et al., 2015).

To determine the contribution of DIC released from OM degradation in the upper reach (f_{UP}), a simple $\delta^{13}C$-based two end-member mixing model was used,

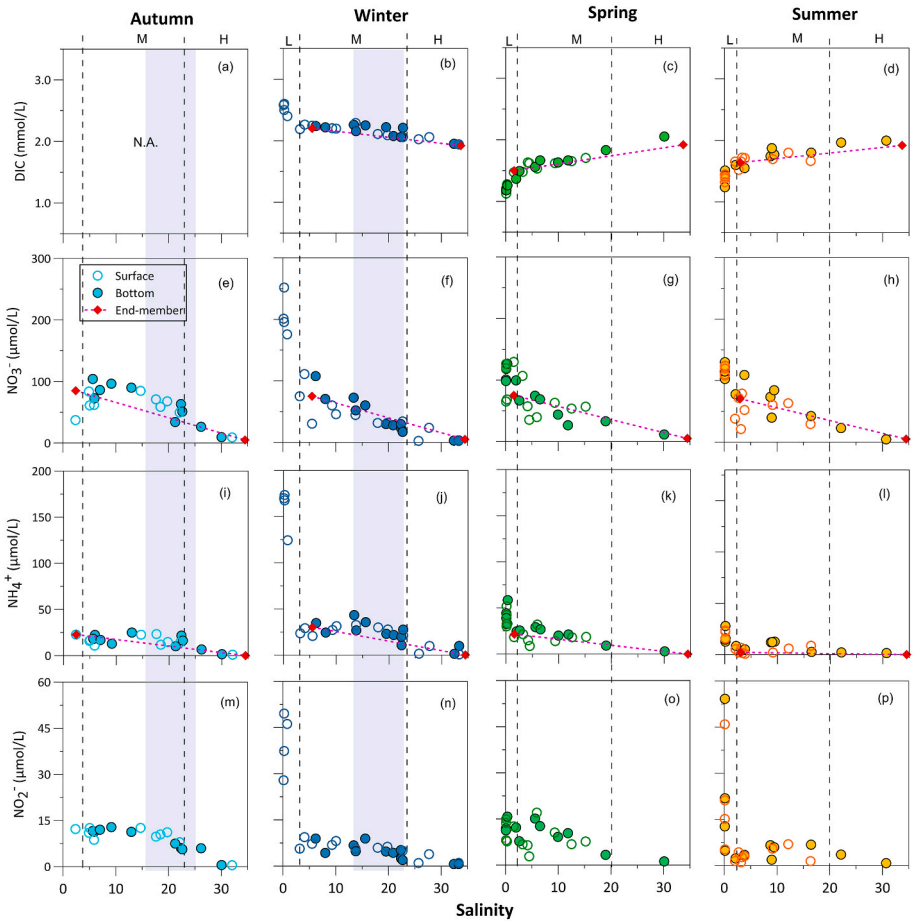

Fig. 6. The concentrations of DIC, NO_3^-, NH_4^+ and NO_2^- in surface and bottom waters versus salinity in the PRE. L, M, and H indicate the low-salinity, intermediate salinity and high-salinity waters. The dashed lines illustrate calculated conservative mixing between the riverine and marine end-members represented by red stars. For definitions of end-member values (stars) see 'Materials and methods'. The turbidity mixing zone is indicated by the gray shaded area.

$$f_{UP}(\%) = (\delta^{13}C_{DICups} - \delta^{13}C_{DICmeas}) / (\delta^{13}C_{DICups} - \delta^{13}C_{DICbio}) \times 100 \quad (9)$$

where $\delta^{13}C_{DICups}$ and $\delta^{13}C_{DICmeas}$ are δ^{13}C-DIC from upstream rivers and those measured in the upper reach. If assuming that (1) OM degradation is the predominant process for the observed DIC variation, and (2) there is minor isotopic fractionation during OM degradation, then, the $\delta^{13}C_{DICbio}$ should inherit the isotopic signal of the OC that consumed oxygen and produced DIC_{bio} (Wang et al., 2016). In this study, we did not measure the effective upstream riverine δ^{13}C-DIC, but rather adopted a value of -10.2 ± 1.1‰ and -8.0 ± 1.2‰ during the wet and dry seasons that has been reported for the Pearl River Delta (Xuan et al., 2020). In fact, the literature data are in good agreement with our estimated effective riverine δ^{13}C-DIC, which can be extrapolated from the non-linear fitting relationship between salinity and δ^{13}C-DIC in the high salinity portion of the estuarine zone to the zero salinity (see Materials and methods). It must be noted that the signal of δ^{13}C-DIC could be strongly influenced by in situ photosynthetic activity in the freshwater of the estuary, especially during winter and summer when high phytoplanktonic biomass (Chl a >20 μg/L) was found (Guo et al., 2015). Therefore, an isotopic correction was required before the δ^{13}C-DIC could be used to evaluation the importance of biotic effects on oxygen dynamics. In order to estimate the fraction of DIC (f_{PP}) converted into organic matter by phytoplankton during photosynthesis, the following two equations are used to distinguish and correct for the effect of phytoplankton DIC uptake on the δ^{13}C-DIC (Esposito et al., 2019),

$$\delta^{13}C_{product} = \delta^{13}C_{input} - \varepsilon_{PP} \times (1 - f_{PP}) \quad (10)$$

where $\delta^{13}C_{product}$ is the δ^{13}C of the accumulated product (i.e., the algal POC), and the term $\delta^{13}C_{input}$ represents the isotopic signatures of DIC before DIC uptake by freshwater phytoplankton. A fixed fractionation factor (ε_{PP}) of 20‰ (with a typical range of 18‰–22‰) was used (Bianchi and Bauer, 2011 and references therein).

For the isotopic signature of the residual DIC pool after phytoplankton DIC uptake,

$$\delta^{13}C_{res} = (\delta^{13}C_{input} + 1000)^*(f_{PP} * \alpha + 1 - f_{PP}) - 1000 \quad (11)$$

where $\alpha = (1000 + \varepsilon_{PP})/1000$.

Based on the measured Chl a concentrations and using the POC/Chl a ratio of 33.0 μg C μg^{-1} Chl a for freshwater phytoplankton in the upper reach of the PRE (Fu et al., 2014), and assuming the DIC uptake by phytoplankton follows the classical Redfield ratio between DIC and organic matter (Equation (1)), we calculated that the fraction of DIC assimilated by phytoplankton accounts for 3–4%, 1–3% and 6–10% of the river water DIC concentrations in winter, spring and summer, respectively. It should be noted that the photosynthetic uptake of DIC decreases to ca. 0% within the estuary. Regarding the effect on the δ^{13}C-DIC in the near freshwater, DIC uptake during photosynthesis causes C isotopic enrichments of 0.6–0.7% in winter, 0.2–0.5% in spring and 1.1–2.1% in summer in the freshwater (i.e., the upper reach) of the PRE. After consideration of the photosynthetic effect, the freshwater δ^{13}C-DIC could be corrected to −9.8‰ to −8.0‰ (average: -9.0 ± 0.8‰), −12.2‰ to −11.3‰ (average: -11.8 ± 0.3‰) and −11.2‰ to −10.3‰ (average: -10.8 ± 0.3‰) during winter, spring and summer respectively (Fig. 5).

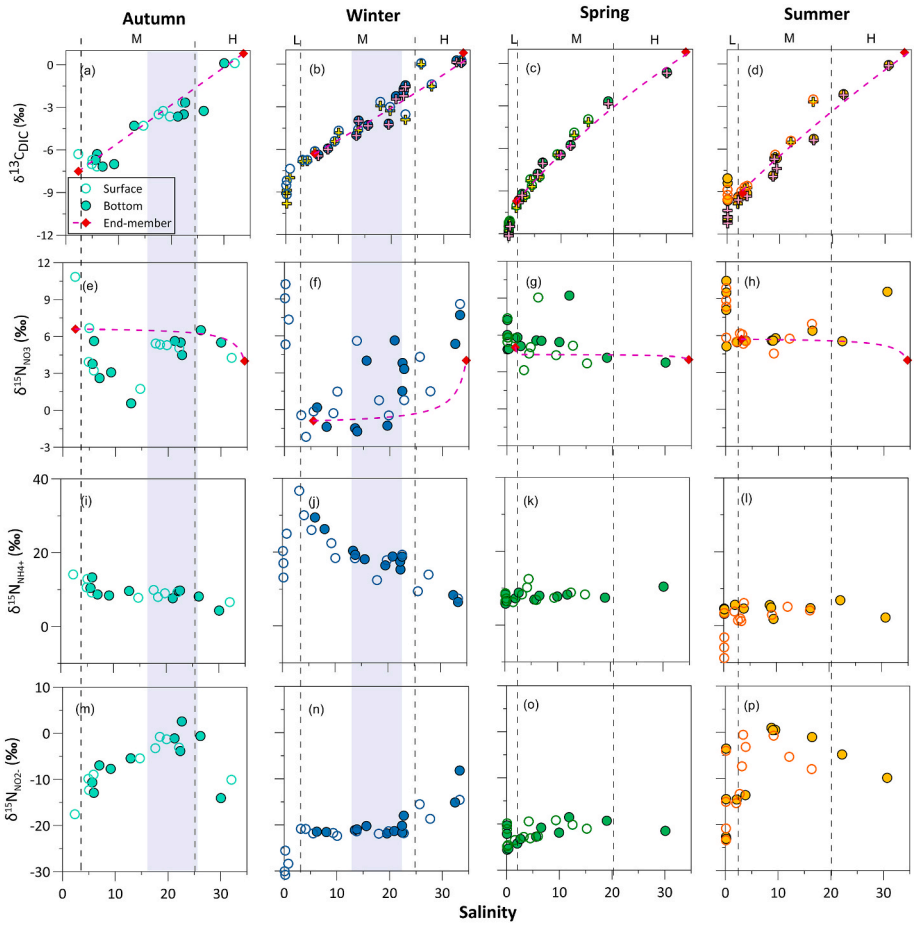

Fig. 7. The isotopic composition of DIC, NO_3^-, NH_4^+ and NO_2^- in surface and bottom waters versus salinity in the PRE. L, M, and H indicate the low-salinity, intermediate salinity and high-salinity waters. The dashed lines illustrate calculated conservative mixing between the riverine and marine end-members represented by red stars. For definitions of end-member values (stars) see 'Materials and methods'. The turbidity mixing zone is indicated by the gray shaded area.

Moreover, taking into account that the variable δ^{13}C-DIC, we therefore used the arithmetic average of the upper reach to calculate the relative contribution of DIC derived from OM degradation. Based on our concurrent δ^{13}C-POC data in the same region, the fraction of DIC derived from OC degradation is estimated to be 4.9 ± 1.7%, 10.2 ± 1.3% and 3.1 ± 1.4% during winter, spring and summer respectively. Using a representative average DIC concentration of 2250, 1480 and 1550 μmol/L in winter, spring and summer respectively, it is estimated that the DIC additions due to aerobic respiration could range from 48.1 ± 21.7 μmol/L to 151 ± 19.2 μmol/L in the upstream waters. If we further assume a −ΔDO/ΔDIC ratio of 1.0–1.3 during OC degradation, as determined in the same region as this study (Zhai et al., 2005; Qian et al., 2018), the corresponding oxygen loss would be 48.1 ± 21.7 μmol/L to 196.3 ± 28.8 μmol/L, which can account for about 44.0 ± 8.3% to 57.2 ± 10.8, 87.5 ± 2.9% to over 100% and 29.1 ± 4.9% to 37.8 ± 6.2% of the corrected apparent oxygen utilization ($AOU_{corrected}$, including AOU and oxygen supplied by photosynthesis) in the upper reach during winter, spring and summer respectively. In contrast, in situ photosynthetic activity by freshwater algae supplies 32.1 ± 4.9%, 12.3 ± 2.5% and 72.9 ± 6.8% of the $AOU_{corrected}$ in winter, spring and summer, respectively.

At the estuarine mixing zone (3 < S < 20) (i.e., the lower section of upper reach and inner estuary during the dry season, and the inner and outer estuary during the wet season), the mixing between the riverine freshwater and seawater dominates the isotopic variability of DIC in the water column, especially in March when there is no significant or small deviations from conservative mixing (Fig. 6). In contrast, the deviation of δ^{13}C-DIC from mixing was considerable in summer, accompanied by significant DIC additions (up to 170 μmol/L) and oxygen consumption, mostly found in the bottom waters. Moreover, substantial POC removal was detected during the same period (Guo et al., 2015). Taken together, these findings suggest the DIC production and oxygen consumption due to OM remineralization via aerobic respiration. Similar to the case in the upper reach, we can simply estimate the contribution of OC degradation to the total DIC pools (f_{MZ}) and the associated oxygen consumption by the following equation:

$$f_{MZ}(\%) = (\delta^{13}C_{DICcons} - \delta^{13}C_{DICmeas}) / (\delta^{13}C_{DICcons} - \delta^{13}C_{DICbio}) \times 100 \quad (12)$$

where $\delta^{13}C_{DICcons}$ and $\delta^{13}C_{DICmeas}$ are the conservative and measured δ^{13}C-DIC values, respectively. Similarly, the $\delta^{13}C_{DICbio}$ is the isotopic composition of additional DIC that is produced by OC mineralization, which should be identical to the δ^{13}C of the OC (Wang et al., 2016).

Based on the existing deviations and the concurrent δ^{13}C-POC data (Guo et al., 2015), we calculated that OC degradation accounts for up to 2.5% of the total DIC pools in the estuarine mixing zone, among which both marine and terrestrial-derived OM could contribute to the DIC additions (Su et al., 2017; Zhao et al., 2020). Also, if we further assume the stoichiometry ratio of 1.0–1.3 for oxygen consumption/DIC addition during OC degradation was applied. Then, the degradation of OC due to aerobic respiration can contribute approximately 48.3–93.5% of the observed oxygen loss in the bottom water during summer. With respect to the outer estuary, in situ photosynthesis, probably from the surface waters, supplies 29.6%–60.7% of the bottom AOU in two sampling sites, while OC degradation consumed 26.9%–89.7% of the bottom AOU in the other two stations.

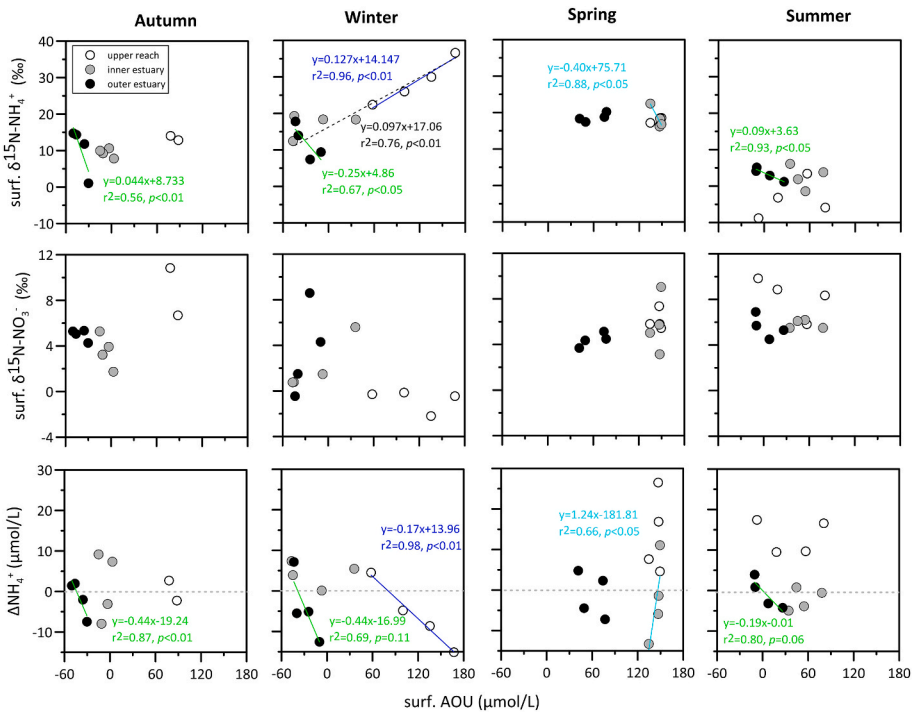

Fig. 8. Relationship between surface water $\delta^{15}N$ of NH_4^+ and AOU (upper panels), $\delta^{15}N$ of NO_3^- and AOU (middle panels) and ΔNH_4^+ versus AOU (lower panels) in different sections of the PRE.

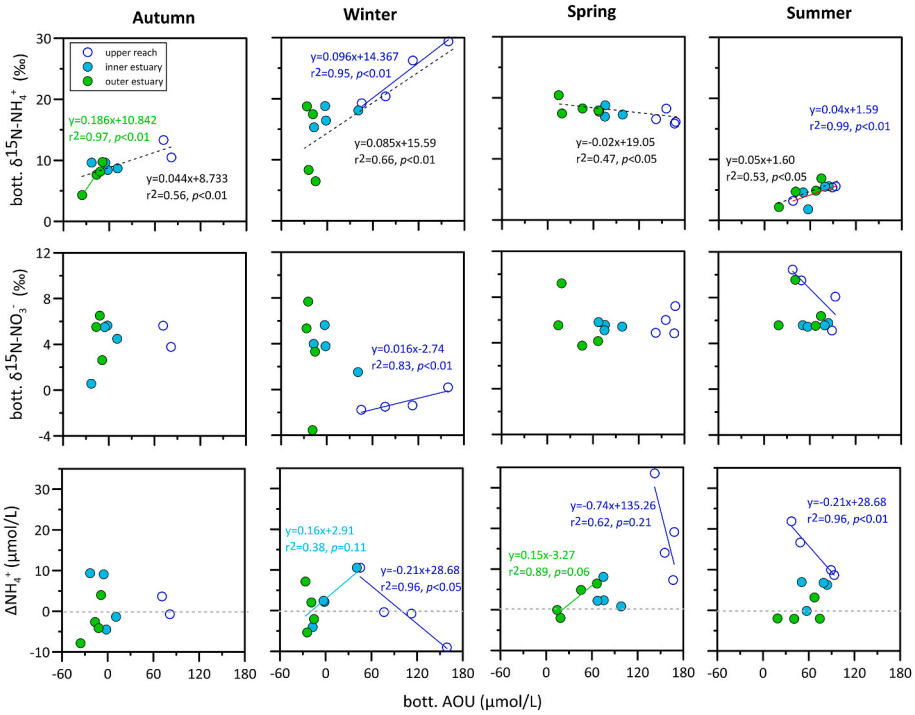

Fig. 9. Relationship between bottom water $\delta^{15}N$ of NH_4^+ and AOU (upper panels), $\delta^{15}N$ of NO_3^- and AOU (middle panels) and ΔNH_4^+ versus AOU (lower panels) in different sections of the PRE.

In the dry periods, we note that the mid-salinity samples (i.e., the inner estuary with salinity range from 10 to 20) have more isotopically depleted DIC than mixing, but associated with fully oxic conditions. This decoupling could be explained by the combined effects of intense physical sediment-water interaction and enhanced air-sea gas exchange due to strong wind mixing. Prior work in the PRE have demonstrated that the sediment-water fluxes of DIC, which inherits the $\delta^{13}C$ signals from bulk sediment/particulate OC being mineralized, are high during the November 2013 sampling cruise (Cai et al., 2015). These isotopically depleted DIC would be diffused into the water column by the enhanced wind-driven mixing in the dry period. The effect of sediment-water interaction is also reflected by the elevated SPM and POC

concentrations (Fig. 3) that paralleled the negative deviations of δ^{13}C-DIC (Fig. 7). On the other hand, the role of atmospheric CO_2 to DIC (add DIC to the system with enriched δ^{13}C) is considered to be minor due to the high partial pressure of CO_2 in the water column (Guo et al., 2009). However, the atmospheric O_2 exchange is active as a result of the wind effect on mixing and the substantial oxygen gradient between the atmosphere and water column (Qian et al., 2018). Thus, high concentrations of DO but more depleted δ^{13}C-DIC were found during the dry period. Nevertheless, the respective role of low oxygen waters liberated from sediments and air-sea O_2 exchange on DO dynamics is difficult to quantify.

4.2. Isotopic evidence of nitrification-induced oxygen depletion

4.2.1. Isotopic evidence for nitrification-induced oxygen consumption

Nitrification is attributed as an important mechanism contributing to O_2 consumption in estuaries and coastal oceans (Déri, 1991; Brion et al., 2000; Dai et al., 2008; Hsiao et al., 2014). For example, it can constitute 20–64% of the total oxygen consumption at the mid-salinity zone of the Mississippi River estuary (Pakulski et al., 1995). Nitrification is a two-step process, where ammonium is oxidized via nitrite to nitrate. The magnitude of the isotope effect for ammonia oxidation (AO), the first step of nitrification, is large (Casciotti et al., 2003). In the second step, nitrite oxidation (NO) will transfer NO_2^- with an inverse but limited isotope effect (Casciotti et al., 2003). As a consequence, the isotopic offset/change between the substrate NH_4^+ and product NO_2^-/ NO_3^- have the potential to be used to assess the relative importance of nitrification on biological N turnover processes (Fripiat et al., 2014; Wells and Eyre, 2019).

To freshwater-dominated estuaries, the spatial distribution of δ^{15}N of NO_3^- and NH_4^+ is largely regulated by mixing between freshwater and seawater (Cifuentes et al., 1989; Wankel et al., 2006; York et al., 2007). However, our work showed that in the low salinity waters, the mixing of multiple riverine inputs is not solely responsible for the overall patterns of δ^{15}N of both NH_4^+ and NO_3^-, indicating other processes such as nitrification must be invoked (see following discussion). Further downstream in the estuarine mixing zone (i.e., the inner estuary) with salinity range from 3 to 20, the freshwater-seawater mixing appears mainly responsible for the spatial patterns of concentrations and isotopic composition of two DIN species (Figs. 6 and 7). In the outer estuary with salinities >20, NO_3^- isotopic composition was mainly controlled by the freshwater-seawater mixing and phytoplankton drawdown (Fig. 7), see details in Ye et al. (2016).

Multiple N processes contribute to variation in concentration and isotopic values of DIN species in the estuarine environments. Among these processes, nitrification and OM degradation/photosynthesis are processes that couples N transformations and oxygen dynamics. In contrast, denitrification, dissimilatory nitrate to ammonium (DNRA) and anaerobic ammonium oxidation (anammox) are anoxic (i.e., the absence of oxygen) and compete for NO_x as electron acceptors. They occur mainly in oxygen-depleted water columns and sediments, and act as the major sinks of fixed N in coastal oceans (Dong et al., 2009; Fernandes et al., 2012; Giblin et al., 2013). However, considering that oxygen concentrations in the water column are usually higher than the anoxic conditions in most hypoxic (<62.5 μmol/L) estuarine systems, these microbial processes should play a minor role in the concentration and isotopic variations of total N pools. Even if we consider the sedimentary N removal processes, previous studies in the PRE have shown that denitrification was the predominant NO_X removal process (>70%–100%), while DNRA and anammox made up only a minor contribution (Tan et al., 2019; Huang et al., 2022). In addition, sedimentary N loss involved mainly particulate organic form deposited onto sediments, with water column derived NO_X acting as the secondary source (Tan et al., 2019). Taken together, we assume that with the exception of nitrification and OM degradation/photosynthesis, other microbial effects are of less importance.

In the upper reach before the mixing of multiple riverine inputs, the δ^{15}N-NH_4^+ increased gradually with increasing AOU during both summer (in bottom waters) and winter (in both surface and bottom waters), whereas the δ^{15}N-NO_3^- showed the opposite trend (Figs. 8 and 9). The decrease in DO concentration was highly coherent and roughly in line with the removal of NH_4^+ but NO_3^- addition (Fig. 6). These covariation trends may be related to nitrification, as it generally adds isotopically light N to the NO_3^- pool whereas the ^{15}N of the residual NH_4^+ pool becomes enriched, due to the significant N isotopic fractionation during NH_4^+ oxidation. Additional evidence confirmed that nitrification dominates N turnover process in the low salinity waters comes from the fact that the δ^{15}N values of NO_2^- were up to 50‰ depleted than that of NH_4^+ in winter (Fig. 7), and δ^{15}N-NH_4^+/ δ^{15}N-NO_2^- negatively/positively correlated with NH_4^+/NO_2^- in summer (Fig. 9). Moreover, a sharp decrease in phosphate concentration (PO_4^{3-}) further precludes the influence of massive sewage effluent during both seasons (data not shown). Dissolved oxygen is essential during nitrification process, as both ammonia oxidation (consumes 1.5 mol O_2 when oxidizing 1 mol of NH_4^+) and nitrite oxidation (consumes 0.5 mol O_2 when oxidizing 1 mol of NO_2^-) would enhance oxygen consumption (EPA, 1993). Therefore, these lines of evidence suggest that nitrification-induced oxygen consumption would contribute to low oxygen conditions within the estuary, which is consistent with previous findings (Dai et al., 2006; Ye et al., 2016).

Thereafter, both NO_3^- and NH_4^+ concentrations decreased sharply near the Humen outlet. Associated with the decrease in DIN concentrations were a significant decrease in δ^{15}N of NO_3^- but there was no obvious trend for δ^{15}N of NH_4^+. This is most likely due to the multiple river inputs or seawater intrusion and their subsequent mixing. For example, the concentration and N isotopic composition of NO_3^- in the lower reaches of the Xijiang, the largest tributary of the Pearl River system, are much lower than that of the Guangzhou reach, particularly in the rainy season (Li et al., 2019).

Further downstream in the inner estuary with low-to-middle salinities (3 < S < 25), both [NO_3^-] and [NH_4^+] generally decreased with increasing salinity, primarily due to the freshwater-seawater mixing. The much higher [NH_4^+] over conservative mixing (Fig. 6) indicates intensive mineralization of POM (in wet seasons) and/or the flux of NH_4^+ from the sediment-water interface re-suspended by physical mixing (in dry seasons), as indicated by the much higher [Chl a] or [SPM] compared to surrounding waters (Fig. 3). In accordance with this pattern, no correlation between δ^{15}N of NH_4^+ and AOU was found in both summer and winter (Figs. 8 and 9), indicating nitrification is not a primary controlling factor of N dynamics. Nitrification often leads to a negative relationship between ΔNH_4^+ and AOU, similar to that in low salinities. However, the relationship between bottom water ΔNH_4^+ and AOU appears to be countrintuitive in the mixing zone (Fig. 9). We speculate that the degradation of OM in bottom waters or from the sediment-water interface re-suspended by physical mixing is largely responsible for these patterns, as both processes would result in oxygen drawdown and nutrients released by mineralization. In fact, the slopes of the regression line for the [NH_4^+]: AOU plot (0.12–0.15) are in good agreement with those reported in the PRE (Zhai et al., 2005; Qian et al., 2018), and within the typical range of stoichiometry (0.07–0.14) during OM degradation via aerobic respiration and/or photosynthesis (Broecker et al., 1985; Krasakopoulou et al., 2005), providing further evidence that nitrification make a minor contribution to bottom oxygen consumption in this study area.

4.2.2. Quantifying the role of nitrification induced oxygen consumption

Note that the complete nitrification is carried out via a combination of two microbial processes with 1.0 mol NO_3^- addition requires 2.0 mol of O_2 consumption (EPA, 1993). If nitrification (ammonia oxidation) is

assumed to be the major sink for NH_4^+, and conditions are inherently dynamic and new substrate is continuously supplied and partially consumed in the case of the upper reach, we can quantitatively estimate the fraction of ammonia oxidation-removed NH_4^+ in the water column (f_{AO}) based on the following open system model (or steady-state; Sigman et al., 2009).

$$\delta^{15}N-NH_{4\ product}^{+}=\delta^{15}N-NH_{4\ initial}^{+}+\varepsilon_{AO}\times(1-f_{AO}) \quad (13)$$

where $\delta_{initial}$ and $\delta_{product}$ denote the initial and product N isotopic composition of NH_4^+, respectively. ε_{AO} is the isotope effect associated with NH_4^+ oxidation.

Based on our formerly determined apparent isotope effects for NH_4^+ oxidation (i.e., 15.3‰ in summer and 23.7‰ in winter respectively, Ye et al., 2016), and the $\delta^{15}N$ variation of NH_4^+ in the upper reach (from −8.8‰ to 3.4‰ and 17‰–36.6‰ in summer and winter, respectively), we estimated that nearly 20% and 17% of the initial NH_4^+ was removed by AO in the water column during summer and winter, and thus fueled the oxygen consumption. If further assuming that 1.5 mol (or 2.0 mol) of O_2 is consumed during NH_4^+ oxidation (or during the complete nitrification process), we can roughly estimate that about 9.3%–12.4% and 26.5%–35.3% of total oxygen consumption occurred via ammonia oxidation/complete nitrification in summer and winter respectively.

In the second step of nitrification (nitrite oxidation, NO), the $\delta^{15}N$ of final NO_3^- product is dependent on $\delta^{15}N$ of the substrate NO_2^- and the associated isotopic fractionation. As noted by Dai et al. (2008), the NH_4^+ oxidation rate was much higher than the NO_2^- oxidation, therefore resulting in NO_2^- accumulations at most sampling stations in the PRE. Hence, it is more desirable to assess the possible impact of nitrite oxidation on oxygen depletion based on NO_2^- isotopes rather than NH_4^+ isotopes. The $\delta^{15}N$ of NO_3^- produced during nitrite oxidation can be estimated based on Eq. (7), defined by Casciotti (2009):

$$\delta^{15}N-NO_{3\ product}^{-}=\delta^{15}N-NO_{2\ substrate}^{-}-\varepsilon_{NO} \quad (14)$$

where ε_{NO} represents the fractionation factor during nitrite oxidation. According to the $\delta^{15}N$ of NO_2^- and the isotope effect associated with nitrite oxidation (−12.8‰) reported by Casciotti (2009), $\delta^{15}N$ of newly produced NO_3^- should be −15.9 ± 1.4‰ and −3.1 ± 1.4‰ in the near freshwater region (S < 1.0) during winter and summer respectively. If we further assumed that nitrite oxidation is the predominant NO_2^- removal process in the upper estuarine waters, as supported by the decrease in $[NO_2^-]$ (Fig. 6). Then, a simple two end-member mixing model for $\delta^{15}N$-NO_3^- can be applied to calculate the relative contribution of nitrite oxidation-derived NO_3^- to the NO_3^- pool, similar to that of $\delta^{13}C$-DIC. Our result indicates that nearly 28.6 ± 2.7% or up to ~31 μmol (19.8 ± 1.1%, ~38.7 ± 2.2 μmol) of the observed NO_3^- during wet (dry) seasons can be attributed to nitrite oxidation in the upper reach, which is very close to the observed NO_3^- addition in the same region (Fig. 6).

Note that nitrification is carried out via the combination of two microbial processes with 1.0 mol NO_3^- addition requires 0.5 mol O_2 consumption during NO_2^- oxidation. In this case, we can simply estimate the relative importance of NO-induced oxygen consumption. Our calculations showed that NO-induced oxygen consumption could account for ca. 19.2 ± 1.8% and 8.8 ± 0.5% of total oxygen loss in the upper reach during summer and winter, respectively. When the effects of ammonia oxidation and nitrite oxidation are combined, nitrification-induced oxygen consumption can account for 35.3%–44.1% and 28.5%–31.6% of the total oxygen consumption in the upper reach during winter and summer respectively. These values are in good agreement with previous findings (Dai et al., 2008; He et al., 2014), which showed that nitrification-induced oxygen consumption can constitute a maximum of one third of the total oxygen loss in the upper reach of the PRE, based on the seasonal distributions of different N forms and in situ nitrification rates.

Further downstream with increasing salinity, a positive relationship was obtained between bottom ΔNH_4^+ and AOU but no significant relationship was found between $\delta^{15}N$-NO_3^- and AOU (Fig. 9). This indicates that the nitrification-induced oxygen consumption may play only a minor role in the overall oxygen loss in the mid and lower estuary, even though we cannot entirely rule out the effects of mineralization and subsequent nitrification of sedimentary OM on oxygen depletion. Similar patterns have also been reported in other large human-perturbed estuaries around the world, such as the Mississippi River plume, the Changjiang Estuary and Westerschelde Estuarine maximum turbidity zone (Soetaert and Herman, 1995; Pakulski et al., 1995; Zhu et al., 2011).

5. Conclusion

In the present study, we developed a new multi-stable isotope approach ($\delta^{13}C$-DIC and $\delta^{15}N$-NH_4^+ and $\delta^{15}N$-NO_3^-) that offer inherent labels to track and evaluate the effects of degradation of OM and nitrification induced oxygen consumption in leading to water column oxygen drawdown in large human-perturbed estuaries. The degradation of OM was responsible for isotopically light DIC additions and oxygen consumption in the water column. Based on a two end-member mixing model calculation for $\delta^{13}C$-DIC and the Redfield stoichiometry, we estimated that the consumption of DO due to OM degradation can account for 29.1 ± 4.9% to over 100% of the total oxygen loss while in situ photosynthesis supplies oxygen in the upper reach, and increased to 48.3%–93.5% in the inner estuary, but varied largely in the outer estuary. In addition, the well coupled signals of $\delta^{15}N$-NH_4^+ and $\delta^{15}N$-NO_3^- and the associated oxygen consumption was evident in the low salinity waters, providing strong evidence for the influence of nitrification, especially during winter and summer. Using a semi-analytical diagnostic approach based on $\delta^{15}N$-NH_4^+, $\delta^{15}N$-NO_3^- and the N isotopic effects during nitrification, we further estimated that at least 28.5%–44.1% of total oxygen loss in the upper reach can be attributed to nitrification-driven oxygen consumption. Further downstream of the estuary, the effect of nitrification on oxygen depletion was minor.

We note that the multi-stable isotope approach, while promising, is still in its infancy. However, there exists the strong potential of combining stable isotope analysis of C and N pools, and in situ measurements of oxygen consumption rates, to evaluate the role of the degradation of OM and nitrification in fueling oxygen consumption in large river-dominated estuaries. In addition, linking isotopic revealed biogeochemical control coupled with physical processes will allow for a better understanding of the development and maintenance of seasonal hypoxia in estuaries and coastal oceans.

Author statement

Roles of authors for this paper are as follows:

Feng Ye (First Author & Corresponding Author): Conceptualization, Methodology, Funding Acquisition, Writing-Original Draft, Review & Editing.

Guodong Jia: Writing-Original Draft, Review & Editing.

Gangjian Wei: Funding Acquisition, Writing-Original Draft, Review & Editing.

Wei Guo: Methodology, Investigation.

Declaration of competing interest

The authors declare that they have no known competing financial interests or personal relationships that could have appeared to influence the work reported in this paper.

Acknowledgments

This work was funded by the Guangzhou Science, Technology and Innovation Commission (201904010431), the Key Special Project for Introduced Talents Team of Southern Marine Science and Engineering Guangdong Laboratory (Guangzhou) (Guangzhou) (GML2019ZD0308), the National Science Foundation of China (42073074), and the Youth Innovation Promotion Association of CAS (2019346). We would like to thank the captain and crews of Yue-DongGuan-Yu 00589. We are also grateful to Shendong Xu and Zhijie Liu for their help with sampling. Reviews and comments from the editor and anonymous reviewers greatly improved the quality of the paper. This is contribution No.IS-3187 from GIG-CAS. The authors declare no competing financial interests.

Appendix A. Supplementary data

Supplementary data to this article can be found online at https://doi.org/10.1016/j.marenvres.2022.105643.

References

Bianchi, T.S., DiMarco, S.F., Cowan Jr., J.H., Hetland, R.D., Chapman, P., Day, J.W., Allison, M.A., 2010. The science of hypoxia in the Northern Gulf of Mexico: a review. Sci. Total Environ. 408, 1471–1484.

Bianchi, T.S., Bauer, J.E., 2011. Particulate organic carbon cycling and transformation. In: Wolanski, E., McLusky, D.S. (Eds.), Treatise on Estuarine and Coastal Science, vol. 5. Academic, pp. 69–117.

Brion, N., Billen, G., Guézennec, L., Ficht, A., 2000. Distribution of nitrifying activity in the seine river (France) from Paris to the estuary. Estuaries 23, 669–682.

Broecker, W.S., Takahashi, T., Takahashi, T., 1985. Sources and flow patterns of deep-ocean waters as deduced from potential temperature, salinity, and initial phosphate concentration. J. Geophys. Res. 90 (C4), 6925–6939.

Cai, P., Shi, X., Hong, Q., Li, Q., Liu, L., Guo, X., Dai, M., 2015. Using $^{224}Ra/^{228}Th$ disequilibrium to quantify benthic fluxes of dissolved inorganic carbon and nutrients into the Pearl River Estuary. Geochem. Cosmochim. Acta 170, 188–203.

Cai, W.J., Dai, M., Wang, Y., Zhai, W., Huang, T., Chen, S., Zhang, F., Chen, Z., Wang, Z., 2004. The biogeochemistry of inorganic carbon and nutrients in the Pearl River estuary and the adjacent Northern South China Sea. Continent. Shelf Res. 24, 1301–1309.

Cai, W.J., Hu, X., Huang, W., Murrell, M.C., Lehrter, J.C., Lohrenz, S.E., Chou, W.C., Zhai, W., Hollibaugh, J.T., Wang, Y., Zhao, P., Guo, X., Gundersen, K., Dai, M., Gong, G.C., 2011. Acidification of subsurface coastal waters enhanced by eutrophication. Nat. Geosci. 4, 766–770.

Casciotti, K.L., Sigman, D.M., Ward, B.B., 2003. Linking diversity and stable isotope fractionation in ammonia-oxidizing bacteria. Geomicrobiol. J. 20, 335–353.

Casciotti, K.L., 2009. Inverse kinetic isotope fractionation during bacterial nitrite oxidation. Geochem. Cosmochim. Acta 73, 2061–2076.

Chen, J.C., Heinke, G.W., Zhou, M.J., 2004. The Pearl River estuary Pollution Project (PREPP). Continent. Shelf Res. 24, 1739–1744.

Cifuentes, L.A., Fogel, M.L., Pennock, J.R., Sharp, J.H., 1989. Biogeochemical factors that influence the stable nitrogen isotope ratio of dissolved ammonium in the Delaware Estuary. Geochem. Cosmochim. Acta 53, 2713–2721.

Cloern, J.E., Canual, E.A., Harris, D., 2002. Stable carbon and nitrogen isotope composition of aquatic and terrestrial plants of the San Francisco Bay estuarine system. Limnol. Oceanogr. 47 (3), 713–729.

Dai, M., Guo, X., Zhai, W., Yuan, L., Wang, B., Cai, P., Tang, T., Cai, W.-J., 2006. Oxygen depletion in the upper reach of the Pearl River Estuary during a winter drought. Mar. Chem. 102 (1/2), 159–169.

Dai, M., Wang, L., Guo, X., Zhai, W., Li, Q., He, B., Kao, S.-J., 2008. Nitrification and inorganic nitrogen distribution in a large perturbed river/estuarine system: the Pearl River Estuary, China. Biogeosciences 5, 1277–1244.

Déri, A., 1991. The role of nitrification in the oxygen depletion of the River Danube. Verh. Int. Verein. Limnol. 24, 1965–1968.

Diaz, R., Rosenberg, R., 2008. Spreading dead zones and consequences for marine systems. Science 321, 926–929.

Dong, L., Su, J., Wong, L.A., Cao, Z., Chen, J.-C., 2004. Seasonal variation and dynamics of the Pearl River plume. Continent. Shelf Res. 24, 1761–1777.

Dong, L.F., Smith, C.J., Papaspyrou, S., Stott, A., Osborn, A.M., Nedwell, D.B., 2009. Changes in benthic denitrification, nitrate ammonification, and anammox process rates and nitrate and nitrite reductase gene abundances along an estuarine nutrient gradient (the Colne Estuary, United Kingdom). Appl. Environ. Microbiol. 75 (10), 3171–3179.

EPA, 1993. Process Design Manual for Nitrogen Removal, EPA/625/R-93/010. U.S. Environmental Protection Agency, Washington, DC, p. 88.

Esposito, M., Achterberg, E.P., Bach, L.T., Connelly, D.P., Riebesell, U., Taucher, J., 2019. Application of stable carbon isotopes in a subtropical North Atlantic mesocosm study: a new approach to assess CO_2 effects on the marine carbon cycle. Front. Mar. Sci. https://doi.org/10.3389/fmars.2019.00616.

Fernandes, S.O., Michotey, V.D., Guasco, S., Bonin, P.C., Bharathi, P.A.L., 2012. Denitrification prevails over anammox in tropical mangrove sediments (Goa, India). Mar. Environ. Res. 74, 9–19.

Fripiat, F., Sigman, D.M., Fawcett, S.E., Rafter, P.A., Weigand, M.A., Tison, J.-L., 2014. New insights into sea ice nitrogen biogeochemical dynamics from the nitrogen isotopes. Global Biogeochem. Cycles 28. https://doi.org/10.1002/2013GB004729.

Fu, Y., Tang, C., Li, J., Zhao, Y., Zhong, W., Zeng, X., 2014. Sources and transport of organic carbon from the Dongjiang river to the humen outlet of the Pearl River, southern China. J. Geogr. Sci. 24, 143–158.

Giblin, A.E., Tobias, C.R., Song, B., Weston, N., Banta, G.T., Rivera-Monroy, V.H., 2013. The importance of dissimilatory nitrate reduction to ammonium (DNRA) in the nitrogen cycle of coastal ecosystems. Oceanography 26 (3), 124–131.

Guo, W., Ye, F., Xu, S., Jia, G., 2015. Seasonal variation in sources and processing of particulate organic carbon in the Pearl River estuary, South China. Estuar. Coast Shelf Sci. 167, 540–548.

Guo, X., Cai, W.J., Zhai, W., Dai, M., Wang, Y., Chen, B., 2008. Seasonal variations in the inorganic carbon system in the Pearl River (Zhujiang) estuary. Continent. Shelf Res. 28, 1424–1434.

Guo, X., Dai, M., Zhai, W., Cai, W.J., Chen, B., 2009. CO_2 flux and seasonal variability in a large subtropical estuarine system, the Pearl River Estuary, China. J. Geophys. Res. 114, G03013 https://doi.org/10.1029/2008JG000905.

Harrison, P.J., Yin, K., Lee, J.H.W., Gan, J., Liu, H., 2008. Physical-biological coupling in the Pearl River estuary. Continent. Shelf Res. 28, 1405–1415.

He, B., Dai, M., Zhai, W., Guo, X., Wang, L., 2014. Hypoxia in the upper reaches of the Pearl River estuary and its maintenance mechanisms: a synthesis based on multiple year observation during 2000−2008. Mar. Chem. 167, 13–24.

Hsiao, S.S.-Y., Hsu, T.-C., Liu, J., Xie, X., Zhang, Y., Lin, J., Wang, H., Yang, J.-Y.T., Hsu, S.-C., Dai, M., Kao, S.-J., 2014. Nitrification and its oxygen consumption along the turbid Chang Jiang River plume. Biogeosciences 11, 2083–2098.

Huang, F., Lin, X., Yin, K., 2022. Effects of marine produced organic matter on the potential estuarine capacity of NOx removal. Sci. Total Environ. 812, 151471.

Krasakopoulou, E., Souvermezoglou, E., Minas, H.J., Scoullos, M., 2005. Organic matter stoichiometry based on oxygen consumption-nutrients regeneration during a stagnation period in Jabuka Pit (middle Adriatic Sea). Continent. Shelf Res. 25, 127–142.

Li, C., Li, S.-L., Yue, F.-J., Liu, J., Zhong, J., Yan, Z.-F., Zhang, R.-C., Wang, Z.-J., Xu, S., 2019. Identification of sources and transformations of nitrate in the Xijiang River using nitrate isotopes and Bayesian model. Sci. Total Environ. 646, 801–810.

Li, D., Zhang, J., Huang, D., Wu, Y., Liang, J., 2002. Oxygen depletion off the Changjiang (Yangtze river) estuary. Sci. China (Series D) 45 (12), 1137–1146.

Liu, Q.X., Huang, X.P., Zhang, X., Zhang, L., Ye, F., 2012. Distribution and sources of particulate organic carbon in the Pearl River Estuary in summer 2010. Acta Ecol. Sin. 32, 4403–4412 (in Chinese with English abstract).

McIlvin, M.R., Altabet, M.A., 2005. Chemical conversion of nitrate and nitrite to nitrous oxide for nitrogen and oxygen isotopic analysis in freshwater and seawater. Anal. Chem. 77, 5589–5595.

Middelburg, J.J., Levin, L.A., 2009. Coastal hypoxia and sediment biogeochemistry. Biogeosciences 6, 1273–1293.

Ning, X., Lin, C., Hao, Q., Liu, C., Le, F., Shi, J., 2009. Long term changes in the ecosystem in the northern South China Sea during 1976−2004. Biogeosciences 6, 2227–2243.

Pakulski, J.D., Benner, R., Amon, R., Eadie, B., Whitledge, T., 1995. Community metabolism and nutrient cycling in the Mississippi River plume-evidence for intense nitrification at intermediate salinities. Mar. Ecol. Prog. Ser. 117, 207–218.

Qian, W., Gan, J., Liu, J., He, B., Lu, Z., Guo, X., Wang, D., Guo, L., Huang, T., Dai, M., 2018. Current status of emerging hypoxia in a eutrophic estuary: the lower reach of the Pearl River Estuary, China. Estuar. Coast Shelf Sci. 205, 58–67.

Rabalais, N.N., Turner, R.E., Díaz, R.J., Justić, D., 2009. Global change and eutrophication of coastal waters. ICES J. Mar. Sci. 66 (7), 1528–1537.

Rabouille, C., Conley, D.J., Dai, M.H., Cai, W.-J., Chen, C.T.A., Lansard, B., Green, R., Yin, K., Harrison, P.J., Dagg, M., McKee, B., 2008. Comparison of hypoxia among four river-dominated ocean margins: the Changjiang (Yangtze), Mississippi, Pearl, and Rhône rivers. Continent. Shelf Res. 28, 1527–1537.

Redfield, A.C., Ketchum, B.H., Richards, F.A., 1963. The influence of organisms on the composition of seawater. In: Hill, M.N. (Ed.), The Sea. John Wiley, New York, pp. 26–77.

Sigman, D.M., Karsh, K.L., Casciotti, K.L., 2009. Ocean progress tracers: nitrogen isotopes in the ocean. In: Steele, J.H., Turekian, K.K., Thorpe, S.A. (Eds.), Encyclopedia of Ocean Science, second ed. Elsevier, Amsterdam, pp. 4138–4153.

Soetaert, K., Herman, P.M.J., 1995. Nitrogen dynamics in the Westerschelde Estuary (SW Netherlands) estimated by means of the ecosystem model MOSES. Hydrobiologia 311, 225–246.

Strauss, J., Grossman, E.L., DiMarco, S.F., 2012. Stable isotope characterization of hypoxia-susceptible waters on the Louisiana shelf: tracing freshwater discharge and benthic respiration. Continent. Shelf Res. 47, 7–15.

Strickland, J.D.H., Parsons, T.R., 1972. A practical handbook of seawater analysis. Fish. Res. Board Can. Bull. 167, 311.

Su, J., Dai, M., He, B., Wang, L., Gan, J., Guo, X., Zhao, H.D., Yu, F., 2017. Tracing the origin of the oxygen-consuming organic matter in the hypoxic zone in a large eutrophic estuary: the lower reach of the Pearl River Estuary, China. Biogeosciences 14, 4085–4099.

Sun, J., Lin, B., Li, K., Jiang, G., 2014. A modelling study of residence time and exposure time in the Pearl River Estuary, China. J. Hydro-environ. Res. 8, 281–291.

Tan, E., Zou, W., Jiang, X., Wan, X., Hsu, T.-C., Zheng, Z., Chen, L., Xu, M., Dai, M., Kao, S., 2019. Organic matter decomposition sustains sedimentary nitrogen loss in the Pearl River Estuary, China. Sci. Total Environ. 648, 508–517.

Taylor, G.T., Way, J., Scranton, M.I., 2003. Planktonic carbon cycling and transport in surface waters of the highly urbanized Hudson River estuary. Limnol. Oceanogr. 48, 1779–1795.

Testa, J.M., Kemp, W.M., 2012. Hypoxia-induced shifts in nitrogen and phosphorus cycling in Chesapeake Bay. Limnol. Oceanogr. 57, 835–850.

Vaquer-Sunyer, R., Duarte, C.M., 2008. Thresholds of hypoxia for marine biodiversity. Proc. Natl. Acad. Sci. U.S.A. 105, 15452–15457.

Wang, H., Dai, M., Liu, J., Kao, S.-J., Zhang, C., Cai, W.-J., Wang, G., Qian, W., Zhao, M., Sun, Z., 2016. Eutrophication-driven hypoxia in the East China sea off the Changjiang estuary. Environ. Sci. Technol. 50, 2255–2263.

Wankel, S.D., Kendall, C., Francis, C.A., Paytan, A., 2006. Nitrogen sources and cycling in the San Francisco Bay Estuary: a nitrate dual isotopic composition approach. Limnol. Oceanogr. 51, 1654–1664.

Wells, N.S., Eyre, B.D., 2019. $\delta^{15}N$ patterns in three subtropical estuaries show switch from nitrogen "reactor" to "pipes" with increasing degradation. Limnol. Oceanogr. 64, 860–876.

Wu, C., Ji, C., Shi, B., Wang, Y., Gao, J., Yang, Y., Mu, J., 2019. The impact of climate change and human activities on streamflow and sediment load in the Pearl River basin. Int. J. Sediment Res. 34, 307–321.

Wu, Y., Zhang, J., Li, D.J., Wei, H., Lu, R.X., 2003. Isotope variability of particulate organic matter at the PN section in the East China Sea. Biogeochemistry (Dordr.) 65, 31–49.

Xuan, Y., Cao, Y., Tang, C., Li, M., 2020. Changes in dissolved inorganic carbon in river water due to urbanization revealed by hydrochemistry and carbon isotope in the Pearl River Delta, China. Environ. Sci. Pollut. Res. 27, 24542–24557.

Ye, F., Huang, X., Shi, Z., Liu, Q., 2013. Distribution characteristics of dissolved oxygen and its affecting factors in the Pearl River Estuary during the summer of the extremely drought hydrological year 2011. Environ. Sci. 34, 707–714 (in Chinese with English abstract).

Ye, F., Jia, G., Xie, L., Wei, G., Xu, J., 2016. Isotope constraints on seasonal dynamics of dissolved and particulate N in the Pearl River Estuary, south China. J. Geophys. Res. Oceans 121, 8689–8705.

Yin, K., Lin, Z., Ke, Z., 2004. Temporal and spatial distribution of dissolved oxygen in the Pearl River Estuary and adjacent coastal waters. Continent. Shelf Res. 24, 1935–1948.

York, J.K., Tomasky, G., Valiela, I., Repeta, D.J., 2007. Stable isotopic detection of ammonium and nitrate assimilation by phytoplankton in the Waquoit Bay estuarine system. Limnol. Oceanogr. 52, 144–155.

Zhai, W., Dai, M., Cai, W.-J., Wang, Y., Wang, Z., 2005. High partial pressure of CO_2 and its maintaining mechanism in a subtropical estuary: the Pearl River estuary, China. Mar. Chem. 93, 21–32.

Zhang, H., Li, S., 2010. Effects of physical and biogeochemical processes on the dissolved oxygen budget for the Pearl River Estuary during summer. J. Mar. Syst. 79, 65–88.

Zhang, L., Altabet, M.A., Wu, T., Hadas, O., 2007. Sensitive measurement of NH_4^+ $^{15}N/^{14}N$ ($\delta^{15}NH_4^+$) at natural abundance levels in fresh and saltwaters. Anal. Chem. 79, 5297–5303.

Zhang, S., Lu, X.X., Higgitt, D.L., Chen, C.T.A., Han, J., Sun, H., 2008. Recent changes of water discharge and sediment load in the Zhujiang (Pearl River) Basin, China. Global Planet. Change 60, 365–380.

Zhao, Y., Liu, J., Uthaipan, K., Song, X., Xu, Y., He, B., Liu, H., Gan, J., 2020. Dynamics of inorganic carbon and pH in a large subtropical continental shelf system: interaction between eutrophication, hypoxia, and ocean acidification. Limnol. Oceanogr. 65, 1359–1379.

Zhu, Z., Zhang, J., Wu, Y., Zhang, Y.Y., Lin, J., Liu, S.M., 2011. Hypoxia off the Changjiang (Yangtze River) Estuary: oxygen depletion and organic matter decomposition. Mar. Chem. 125, 108–116.